*Proceedings of the 19th Annual Meeting of Particle Accelerator Society of Japan*
*October 18 - 21, 2022, Online (Kyushu University)*

**PASJ2022 FROA07**

# ROBUST AND COMPACT DESIGN OF A 30-MW BEAM TRANSPORT LINE FOR AN ACCELERATOR-DRIVEN SUBCRITICAL SYSTEM

B. Yee-Rendon*, Y. Kondo, J. Tamura, K. Nakano, F. Maekawa and S. Meigo
Japan Atomic Energy Agency (JAEA), Tokai, Japan

## Abstract

The Japan Atomic Energy Agency accelerator-driven subcritical system (JAEA-ADS) pursues the reduction of nuclear waste by transmuting minor actinides. JAEA-ADS drives a 30-MW proton beam to a lead-bismuth eutectic (LBE) spallation target to produce neutrons for a subcritical core reactor. To this end, the JAEA-ADS beam transport to the target (BTT) must provide a suitable beam profile and stable beam power to the beam window of the spallation target to avoid high-thermal stress in the target and reactor components. The JAEA-ADS BTT was optimized by tracking a large number of macroparticles to mitigate the beam loss in the region outside the reactor, performance with high stability in the presence of errors, and fulfill the length requirement. This work presents the design and the beam dynamics studies of the first scheme of the BTT for the JAEA-ADS design.

## INTRODUCTION

The Japan Atomic Energy Agency (JAEA) is developing an accelerator-driven subcritical system (ADS) for the transmutation of the minor actinides [1]. The JAEA-ADS proposal employs a 30-MW proton beam to produce spallation neutrons for an 800-MWth thermal power subcritical reactor, as shown in Fig. 1.
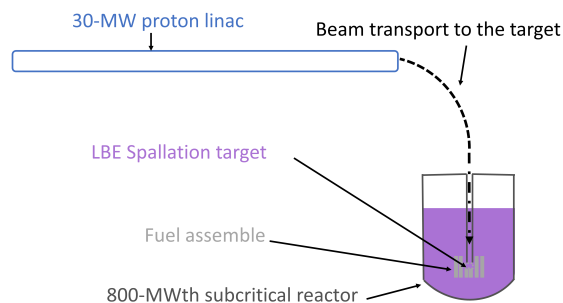


Figure 1: JAEA-ADS scheme.

Once the reference design for the JAEA-ADS linac was established [2], the following step is the design of the beam transport to the target (BTT) that carries out the beam from the end of the linac to the beam windows and onto the spallation target, with a specified beam profile, current density, and beam loss.

The BTT must satisfy the high-reliability operation of the ADS designs; thus, a robust and simple design is pursued. Table 1 presents the main specifications for the BTT based on

the JAEA-ADS subcritical reactor design requirements [3,4]. In addition, the BTT must ensure the integrity of the beam window by providing a low peak current density to avoid excessive head load at the beam window [5]. This work presents a short summary of the design criteria and the beam dynamics performance of a BTT for the JAEA-ADS design. The completed study has been published in Ref [6].

Table 1: Main Characteristics of the Beam Transport to the Target for the JAEA-ADS Proposal

| Parameter | |
|---|---|
| Particle | Proton |
| Beam current (mA) | 20 |
| Beam energy (GeV) | 1.5 |
| Beam power (MW) | 30 |
| Beam loss outside the reactor part (W/m) | < 1 |
| Beam power stability | $\pm$ 1% |
| Beam energy stability | $\pm$ 1% |
| Peak current density ($\mu$A/mm$^2$) | < 0.3 |
| Footprint stability at the beam window | better than $\pm$ 10% |
| Final beam pipe aperture(mm) | < 450 |
| Length (m) | $\approx$ 27 |

## LATTICE DESIGN

The JAEA-ADS BTT must transport a 30-MW beam from the end of the linac to the beam window with a low peak current density, high stability, and reliability. Besides the requirements of beam performance, the BTT must satisfy other specifications, such as its length must be compatible with the footprint of the design, 27 m [3, 4]. In addition, to facilitate the exchanging work during the beam window and fuel replacement, the dipole apertures were chosen to be 100 m to reduce the dipole weight, but this demands a well-focused beam on the transverse plane to avoid beam loss. Therefore, we adopted a simple compact design using normal conducting dipoles and quadrupoles. By using a simple design, we avoided complex arrangements using nonlinear optics that are prone to error, thus affecting its stability.

The BTT is divided into two sections: the beam optics part, where the beam manipulations occur, and the reactor zone, from the upper shield of the subcritical reactor until the beam windows, as shown in Fig. 2. The beam optics section is subdivided into matching, bending, and final focusing regions. Table 2 presents the parameters of the magnets that composed the BTT. The matching section comprises four quadrupoles that accept the beam from the linac and manipulate it to achieve adequate beam parameters for the bending part. The bending sector is an achromatic lattice of

*Proceedings of the 19th Annual Meeting of Particle Accelerator Society of Japan*
*October 18 - 21, 2022, Online (Kyushu University)*

**PASJ2022 FROA07**

two 45° dipoles and two quadrupoles to avoid the increase of the vertical size because of the dispersion. Finally, the focusing section handles the beam to achieve the required beam profile at the beam window by employing five quadrupoles. The BTT has a correction scheme composed of steering magnets and beam position monitors to control the beam centroid along the optics section. In addition, multi-wire or luminescence monitors will be placed to survey the size and position of the beam at the beam windows.
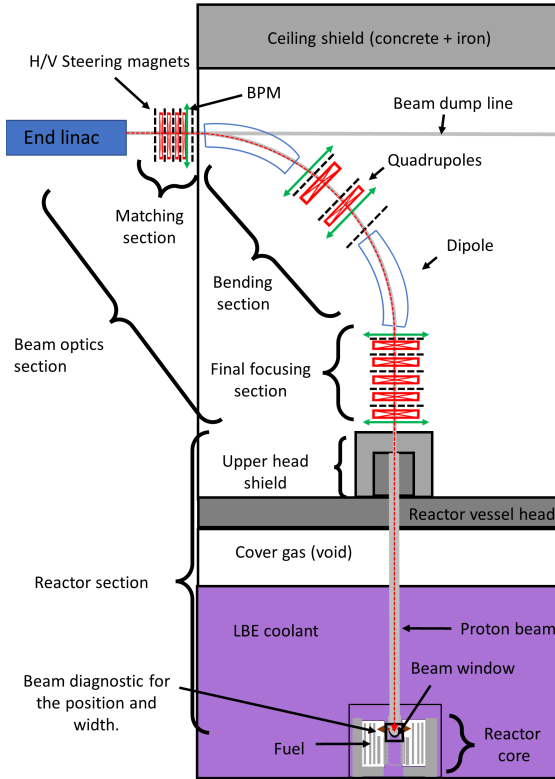


Figure 2: Schematic layout of the BTT for the JAEA-ADS based on subcritical reactor studies [4].

## BEAM DYNAMICS STUDIES

We performed the beam dynamics studies using the TraceWin program [7]. The input distribution was obtained from the JAEA-ADS linac beam tracking simulations [2], which comprised over $9 \times 10^6$ macroparticles. As a first part of this work, the lattice parameters were optimized to achieve a peak current density not higher than the accepted Gaussian profile [5]. A smoothly beam scrapping was implemented to prevent significant perturbations in the beam core, ensure beam control, and minimize the increase of beam loss to guarantee the requirement of beam power at the beam window. Figure 3(a) and (b) show the transverse root-mean-square (rms) beam size. The BTT is achromatic, as is confirmed by the dispersion plot in Fig. 3(c). Figure 4 displays the maximum radial beam profile for the baseline case, the solid red line. The radial envelope is well controlled inside the beam optics section to avoid beam losses and smoothly expands inside the reactor.

Table 2: Magnet parameters that composed the beam transport to the target. For the quadrupoles, the gradient is presented. The positive sign in the quadrupole gradients indicates that the beam is focused on the *x* direction.

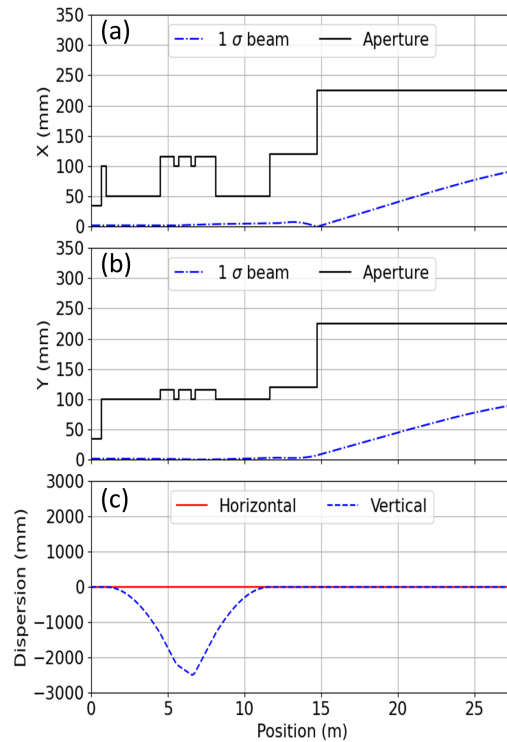| Element | Length (mm) | Gradient (MW)/ Bfield (T) |
|---------|-------------|---------------------------|
| Quad1 | 80 | 11.69 |
| Quad2 | 80 | -2.52 |
| Quad3 | 80 | -1.08 |
| Quad4 | 80 | -13.99 |
| Dipole1 | 3543 | 1.60 |
| Quad5 | 300 | -13.01 |
| Quad6 | 300 | 1.58 |
| Dipole2 | 3543 | 1.60 |
| Quad7 | 300 | -12.55 |
| Quad8 | 300 | 4.55 |
| Quad9 | 300 | 14.79 |
| Quad10 | 300 | 14.99 |
| Quad11 | 300 | 14.85 |



Figure 3: Horizontal (a) and vertical (b) rms beam size and the dispersion function (c) along the BTT.

The radial beam profile from this study exhibits a slightly lower peak current than the Gaussian model around the beam center, as shown in Fig. 5. The low current density at the center is helpful in reducing the thermal stress and increasing

*Proceedings of the 19th Annual Meeting of Particle Accelerator Society of Japan*
*October 18 - 21, 2022, Online (Kyushu University)*
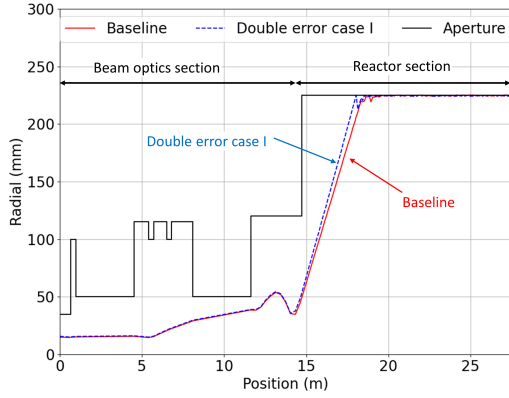
**PASJ2022 FROA07**

Figure 4: Comparison of the maximum radial envelope between the baseline (red solid line) and the double error case I (blue dotted line) along the BTT.

the buckling pressure at the top of the beam windows within a radius of 25 mm. Thus, it is expected that this beam profile will satisfy the feasible conditions of the beam windows. The beam current density presents small fluctuations toward the beam center that are attributed to statistical errors because of the smaller counting area.
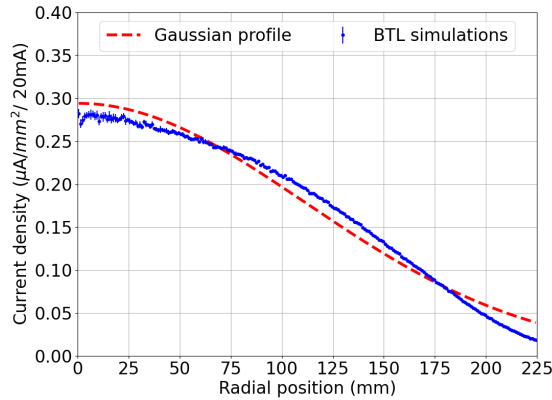


Figure 5: Radial current density at the beam window obtained from the beam tracking simulations and the accepted Gaussian profile [5]. The error bar is proportional to the square root of the proton number counted in each bin.

The accepted Gaussian model scrapes about 13% of the beam. Consequently, the beam current should be increased by the same amount to guarantee the 30-MW at the beam window surface. For our model, 4.8% of the beam is scraped before reaching the beam windows. Thus, our model has the advantage of only requiring an increase of beam current of one-third regarding the Gaussian model.

The second part comprised the evaluation of the robustness and estimation of the tolerances for the BTT design. To this end, we applied beam error studies using a similar proceeding to the JAEA-ADS linac error studies [2]. The errors applied in this study were element errors, e.g., misalignment of quadrupoles, and input beam errors, which are

fluctuations in the beam delivered by the JAEA-ADS linac because of baseline operation and fast recovery schemes. In addition, the errors were divided into static and dynamic errors. The former remain constant for long periods; thus, they can be measured and corrected. The latter are random errors, therefore, stay uncompensated.

Table 3: Summary of the Static Element Errors for the Beam Transport to the Target

| Element | Quadrupole | Dipole |
|---|---|---|
| $\Delta x, \Delta y$ [8] (mm) | 0.45 | 0.5 |
| $\Delta \theta x, \Delta \theta_y$ [9](mrad) | 1.2 | 2.4 |
| $\Delta \theta_z$ (mrad) | 6 | 2.4 |
| Magnet field (%) | 0.5 | 0.05 |

Table 4: Summary of the Dynamic Element Errors for the Beam Transport to the Target

| Element | Quadrupole | Dipole |
|---|---|---|
| $\Delta x, \Delta y$ (mm) | 0.01 | 0.01 |
| $\Delta \theta x, \Delta \theta_y$ (mrad) | 0.01 | 0.02 |
| $\Delta \theta_z$ (mrad) | 0.06 | 0.02 |
| Magnet field (%) | 0.05 | 0.005 |

Tables 3 and 4 summarize the element errors. Their amplitudes were defined based on other error studies [2, 10] and corrected to achieve the demanded stability presented in Table 1. Table 5 presents the input beam errors. For the static case, we used the results of the fast recovery compensation studies for the JAEA-ADS linac, which are rematched schemes to enable a fast-stable linac operation recovery with an acceptable beam quality to achieve high availability in case of a faulty element [11]. The cases were classified according to the type of failure in single superconducting radiofrequency cavities (SSRFC), multiple superconducting radiofrequency cavities (MSRFC), and magnets (Mag) failures. The amplitudes presented in the table are increased by 20% to increase the severity of the cases.

Table 5: Summary of the Input Beam Errors for the BTT

| Parameters | SSRFC | MSRFC | Magnet | Dynamic |
|---|---|---|---|---|
| $\Delta x, \Delta y$ (mrad) | 1 | 1 | 1 | 0.02 |
| $\Delta \phi$ ((deg)) | 1 | 1 | 1 | 0.02 |
| $\Delta x', \Delta y'$ (mrad) | 1 | 1 | 1 | 0.02 |
| $\Delta$ Beam energy (keV) | 0.4 | 0.4 | 0.4 | 0.1 |
| $(\Delta \epsilon / \epsilon_0)_t$ [12] (%) | 4 | 28 | 27 | 1 |
| $(\Delta \epsilon / \epsilon_0)_l$ (%) | 28 | 192 | 21 | 1 |
| $M_t$ (%) [13] | 5 | 15 | 14 | 1 |
| $M_l$ (%) | 11 | 28 | 14 | 1 |

We applied double errors consisting of the simultaneous application of the element and the input beam errors. The errors were separated into static and dynamic cases, as shown

*Proceedings of the 19th Annual Meeting of Particle Accelerator Society of Japan*
*October 18 - 21, 2022, Online (Kyushu University)*

**PASJ2022 FROA07**

in Table 6. Each double error case comprised 1,000 independent runs with a beam distribution of $9 \times 10^6$ macroparticles. In each run, the amplitude error is assigned independently and uniformly plus-minus the maximum value presented in Tables 3, 4, and 5.

Table 6: Double Error Description

| Case | Type | Definition |
|------|------|------------|
| I | Static | Element errors + SSRFC input beam errors |
| II | Static | Element errors + MSRFC input beam errors |
| III | Static | Element errors + Mag input beam errors |
| IV | Dynamic | Element errors + input beam errors |

Figure 6 shows the difference in beam power for each run of the double error case I regarding the baseline. In addition, Fig. 4 compares the average maximum radial envelope of the double error case I against the baseline. The study reveals that the beam performance for both cases was similar, indicating an adequate beam stability.
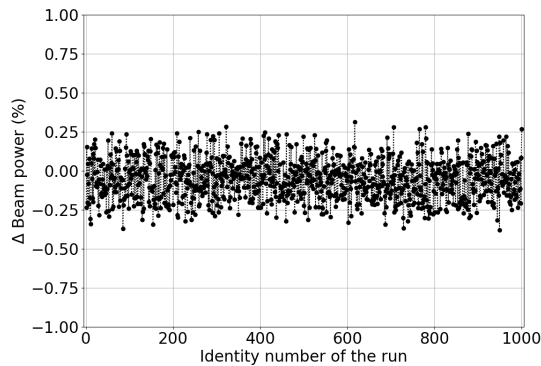


Figure 6: Beam power fluctuations to the baseline for double error case I.

Figure 7 summarizes the beam performance of the double errors with a confidence level of 99%. All the beam losses were confined inside the reactor part. Figure 7(a) shows the beam energy is lower than $\pm 7.5$ MeV, equivalent to 0.5% of the baseline beam energy. The beam power fluctuations are inside $\pm 1\%$, as shown in Fig. 7(b). Figures 7(c) and (d) display the rms size growth is below $\pm 6\%$, and the transverse offset is within $\pm 9$ mm, respectively. The dynamics offset will be removed using active beam correction from the beam position observed by the instrument placed at the beam windows.
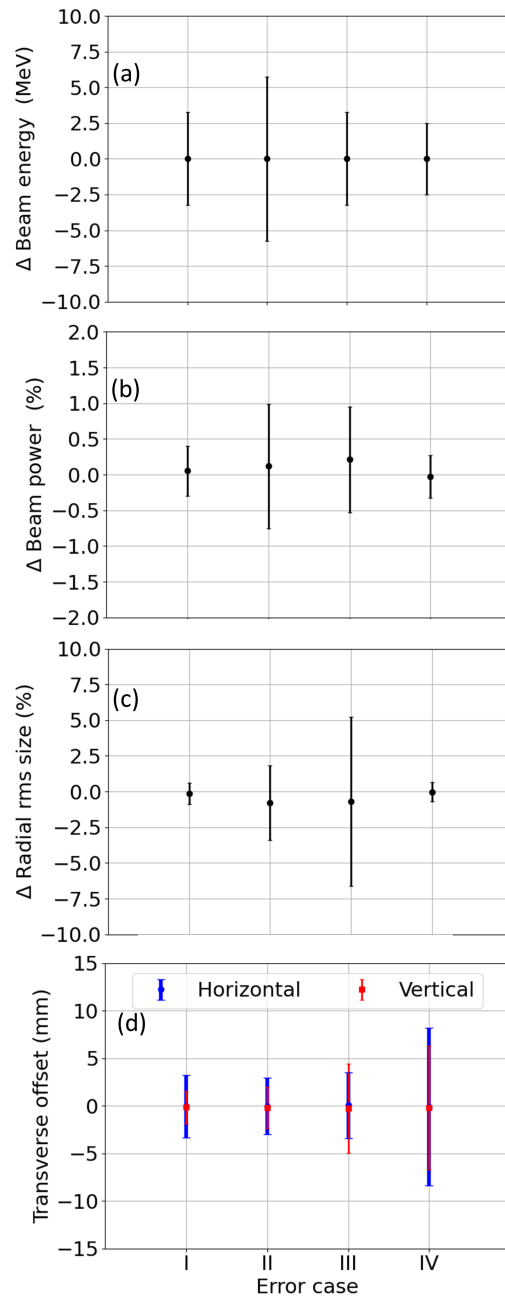


Figure 7: Summary of the beam error degradation for different error cases defined in Table. The plot (a) is the difference in kinetic energy, (b) beam power, (c) radial rms size, and (d) transverse offset. The error bars denote 2.57 standard deviation, for a 99% confidence interval.

## CONCLUSIONS

This work discusses the design and presents the beam dynamics studies of the beam transport to the target for the JAEA-ADS proposal. The JAEA-ADS BTT must properly transport a 30-MW beam from the end of the linac to the beam windows and onto the spallation target while fulfilling stringent conditions of beam stability and engineering specifications. The design provides an efficient beam profile at the beam windows with low peak current density to satisfy the feasibility of the beam windows and small beam scraping, which reduces the extra beam power required. This study applied double errors that comprise input beam and element errors to investigate the viability of the fast-recovery compensation schemes, which are crucial strategies to operate with high reliability, and set up the element tolerances. The

Proceedings of the 19th Annual Meeting of Particle Accelerator Society of Japan
October 18 - 21, 2022, Online (Kyushu University)

PASJ2022 FROA07

analysis confirms that the BTT design meets the stringent beam window stability of the JAEA-ADS.

## ACKNOWLEDGMENTS

## REFERENCES

[1] T. Sugawara *et al.*, "Research and Development Activities for Accelerator-Driven System in Jaea", *Prog. Nucl. Energy*, vol. 106, p. 27, Feb. 2018. `doi:10.1016/j.pnucene.2018.02.007`

[2] B. Yee-Rendon *et al.*, "Design and beam dynamic studies of a 30-MW superconducting linac for an accelerator-driven subcritical system", *Phys. Rev. Accel. Beams.*, vol. 24, p. 120101, Dec. 2021. `doi:10.1103/PhysRevAccelBeams.24.120101`

[3] T. Sugawara and K. Nishihara, private communication, Nov. 2021.

[4] H. Iwamoto *et al.*, "Radiation shielding analysis of the upper structure of an accelerator-driven system", JAEA, Tokai, Japan,Rep. JAEA-Research 2021-012, Dec. 2021 (Japanese).

[5] T. Sugawara *et al.*, "Conceptual Design Study of Beam Window for Accelerator-Driven System", *J. Nucl. Sci. Techol.*, vol. 47, p. 953, May. 2010. `doi:10.1080/18811248.2010.9720974`

[6] B. Yee-Rendon *et al.*, "Beam physics design of a 30-MW beam transport to the target for an accelerator-driven subcritical system", *JINST*, vol. 17, p. P10005, Oct. 2022. `doi.org/10.1088/1748-0221/17/10/P10005`

[7] TraceWin Manual, `http://irfu.cea.fr/dacm/logiciels`

[8] $\Delta x$ and $\Delta y$ are displacement in the horizontal and vertical directions, respectively.

[9] $\Delta \theta_u$ indicates rotation error around the subscript axis of the quadrupole magnets. $u$ is for each axis in the transverse plane and longitudinal axis.

[10] B. Brañas *et al.*, "Design, manufacturing and tests of the LIPAc high energy beam transport line", *Nuc. Fusion.*, vol. 61, p. 1, Sept. 2020. `doi:10.1088/1741-4326/abbba1`

[11] B. Yee-Rendon *et al.*, "Beam dynamics studies for fast beam trip recovery of the Japan Atomic Energy Agency accelerator-driven subcritical system", *Phys. Rev. Accel. Beams*, vol. 25, p. 080101, Aug. 2022. `doi:10.1103/PhysRevAccelBeams.25.080101`

[12] The normalized rms emittance growth with respect to the baseline.

[13] The beam mismatch with respect to the baseline.